The small ribosomal subunit from *Thermus thermophilus* at 4.5 Å resolution: Pattern fittings and the identification of a functional site

Ante Tocilj*, Frank Schlünzen*, Daniela Janell*, Marco Glühmann*, Harly A. S. Hansen*, Jörg Harms*, Anat Bashan†, Heike Bartels*†, Ilana Agmon†, Francois Franceschi‡, and Ada Yonath*†§

*Max Planck Research Unit for Ribosomal Structure, 22603 Hamburg, Germany; †Department of Structural Biology, Weizmann Institute, 76100 Rehovot, Israel; and ‡Max Planck Institute for Molecular Genetics, 14195 Berlin, Germany

Communicated by Alexander Rich, Massachusetts Institute of Technology, Cambridge, MA, September 24, 1999 (received for review August 23, 1999)

The electron density map of the small ribosomal subunit from *Thermus thermophilus*, constructed at 4.5 Å resolution, shows the recognizable morphology of this particle, as well as structural features that were interpreted as ribosomal RNA and proteins. Unbiased assignments, carried out by quantitative covalent binding of heavy atom compounds at predetermined sites, led to the localization of the surface of the ribosomal protein S13 at a position compatible with previous assignments, whereas the surface of S11 was localized at a distance of about twice its diameter from the site suggested for its center by neutron scattering. Proteins S5 and S7, whose structures have been determined crystallographically, were visually placed in the map with no alterations in their conformations. Regions suitable to host the fold of protein S15 were detected in several positions, all at a significant distance from the location of this protein in the neutron scattering map. Targeting the 16S RNA region, where mRNA docks to allow the formation of the initiation complex by a mercurated mRNA analog, led to the characterization of its vicinity.

crystallography of ribosomes | mRNA binding | 30S

Ribosomes are the universal cellular organelles on which protein biosynthesis takes place. They are nucleoprotein assemblies, built of two independent subunits of unequal size that associate on the initiation of protein biosynthesis. The small subunit (0.85 mDa) provides the site for the initiation step and facilitates the decoding of the genetic information. It contains 21 proteins and an RNA chain (16S) of ≈1,500 nucleotides. Significant conformational variability of 30S particles has been observed by cryoelectron microscopy studies (1, 2), by surface probing (3), and by monitoring the ribosomal activity (4).

The inherent flexibility of small ribosomal subunit may be the reason for the low (≈10 Å) resolution of the early crystals of the small ribosomal subunits from *Thermus thermophilus*, T30S (5, 6). It also may account for the unsuitability of all of the available cryoelectron microscopy models of the small ribosomal subunit for extracting initial phase sets, as performed successfully for the large ribosomal subunits (7). Indeed, increasing the homogeneity of the crystallized particles, accompanied by postcrystallization rearrangements, induced by minute amounts of a heteropolytungstate containing 18 W atoms (8), called here W18, resulted in diffraction to 3 Å.

This dramatic increase in crystal quality was not accompanied by changes in the unit cell dimensions or in the crystal symmetry. However, the W18-treated crystals (called Wative) could not be scaled to the original native crystals, suggesting that a major conformational rearrangement occurred upon the W18 treatment. It is conceivable that other metals could have led to a similar effect. Nevertheless, among the many tungsten compounds tested by us (9), only W18 was found suitable for the increase in resolution.

Conformational changes are not routinely induced within crystals because of the limitation of the motion imposed by the crystal network. However, the realization that the T30S crystals can tolerate such changes, prompted us to perform reactivation of the crystallized T30S particles by controlled heating (10). This procedure led to higher proportions of well diffracting crystals and enabled almost quantitative binding of compounds participating in protein biosynthesis or their analogs (1, 11).

Ribosomal crystallography has been found to be rather challenging, especially upon progressing to higher resolution. Consequently, the structure determination proceeds by step-wise approach, progressing from low to higher resolution. Furthermore, most of the interpretations of the currently available electron density maps hinge on models accommodating noncrystallographic structural information (3, 4, 12–19) and exploiting known structures of RNA and of isolated ribosomal proteins. Considerable uncertainties are associated with placements of structures determined at high resolution in medium resolution maps. In the case of the ribosome, special concern is require for minimizing potential ambiguities because its individual components contain common motifs (20, 21). In addition, molecular mimicries (22) may mislead the differentiation between proteins and RNA regions. The non-negligible conformational variability of the ribosomal components (20, 21), accompanied by possible influences of the *in situ* ribosomal environment, may also lead to misinterpretations.

To facilitate unbiased crystallographic identifications, to target sites involved in ribosomal functions, and at the same time to extend the resolution of heavy atom derivatives, we are focusing on the attachment of heavy atom markers to natural or genetically engineered probes at predetermined sites. We also exploit carriers that posses high specific affinities to ribosomal moieties, such as antibiotics or DNA oligomers complementary to exposed RNA regions. In this way, two surface cysteine residues as well as the 3′ end of the 16S RNA have been localized (11, 23, 24). Furthermore, in a few cases, the labeled crystals diffracted to resolution almost matching that of the Wative crystals and yielded data of adequate quality, presumably by reducing the flexibility of the targeted regions.

In this manuscript we present the 4.5 Å map of T30S and show the parts that have been interpreted so far. We focus on strategies and methodologies including the design, choice, and combination of derivatives. We show placements of RNA regions of known motifs as well as of ribosomal proteins of known structures. We also highlight the sites targeted by heavy atom markers, among them an mRNA analog.

Abbreviations: BS crystal, back-soaked crystal; TAMM, tetrakis(acetoxymercuri)-methane.

Data deposition: The atomic coordinates have been deposited in the Protein Data Bank, www.rcsb.org (PDB ID code 1C59).

§To whom reprint requests should be addressed. E-mail: yonath@mpgars.desy.de.

The publication costs of this article were defrayed in part by page charge payment. This article must therefore be hereby marked "*advertisement*" in accordance with 18 U.S.C. §1734 solely to indicate this fact.

Table 1. Phasing statistics

Data set	Unique reflections	Resolution, Å	Completeness (outer shell), %	R_{sym}, %	R_{merge}, %	Phasing power	R_{cullis}	Sites
	Soaking							
BS (Native)	85991	4.5*	93.2 (91.1)	10.8	—	—	—	—
Wative 1	56350	5.0	95.7 (99.6)	13.2	17.9	1.2	0.74	4
Wative 2	68335	4.4	81.5 (80.5)	12.3	16.6	1.5	0.77	3
Wative (anomalous)	42995	7.0	99.1 (99.6)	7.6	17.2	1.6/1.1†	0.4/0.8†	3
Ta_6Br_{14}	46690	6.0	68.0 (44.0)	14.2	26.6	1.4	0.84	3
$Hg_3C_6O_4H_8$‡	17092	6.5	60.1 (58.7)	14.4	22.9	1.3	0.73	7
$C_2Hg_6N_2O_8$	55800	5.9	79.6 (75.0)	6.9	21.7	1.7	0.50	4
PIP	62015	4.5	80.9 (80.3)	14.1	17.5	0.5	0.91	6
K_2O_4Os	49751	5.0	77.9 (84.4)	14.7	22.9	1.0	0.68	7
Pb_3-citrate‡§	26982	6.4	92.4 (75.2)	11.1	14.6	1.1	0.79	8
$NaAuCl_4$	30078	5.5	81.0 (78.0)	13.6	15.5	1.0	0.78	1
W_4	26748	6.4	91.8 (91.3)	11.8	15.0	0.9	0.72	4
K_2PtCl_4‡	23551	6.5	81.5 (78.5)	11.1	20.9	0.8	0.90	7
	Specific covalent binding or hybridization							
oliT‡§	36083	4.8¶	58.1 (60.6)	14.2	14.9	3.1	0.71	1
TAMM	25797	7.0	60.3 (61.5)	10.7	16.4	0.6	0.94	2
TIR‡§	43424	4.5	57.3 (16.3)	8.5	21.4	0.6	0.88	2
Methyl-Hg-acetate‡§	29719	6.0	80.6 (71.9)	13.7	16.2	1.2	0.66	6
Uranyl-acetate‡§	30911	6.0	84.4 (75.1)	12.3	15.3	0.5	0.85	5
	Derivatives with dual chemical properties							
AquaPt	28439	5.0	49.3 (59.3)	15.9	26.1	0.6	0.85	5
CisPt	19366	6.9	80.7 (70.3)	9.9	18.1	0.6	0.84	3

$R_{sym} = \Sigma|I - \langle I\rangle|/\Sigma\langle I\rangle$, $R_{merge} = \Sigma|F_{PH} - F_P|/\Sigma F_P$, $R_{cullis} = \langle$phase-integrated lack of closure$\rangle/\langle|F_{PH} - F_P|\rangle$, Phasing power $= \langle[|F_H(calc)|/$phase-integrated lack of closure$]\rangle$. PIP, diiodopiplatinum (II) diethyleneamine; W_4, (tetramethylammonium)$_2Na_2[Nb_2W_4O_{14}18H_2)]$; TIR, a tetrairidium cluster; aquaPt, *cis*-diaquacisplatin; cisPt; *cis*-$[Pt(NH_3)_4]$.

*Data were collected to 3 Å, but not used in this study.

†iso/ano.

‡SIR, not incorporated yet.

§Wative was considered as native.

¶Data were collected to 3.5 Å, but not used in this study.

Materials and Methods

Crystal Preparation. Ribosomal subunits from *T. thermophilus* were prepared and crystallized as described (5, 23). The crystals ($a = b = 407$ Å, $c = 176$Å, $P4_12_12$, hand determined from anomalous data) were treated by the addition of millimolar amounts of W18. Back-soaked (BS) crystals were generated by soaking the W18-treated crystals (Wative) in their stabilization solution for 10–40 hours. The content of W18 in the BS crystals was determined as described (9). Derivatization was performed by soaking the Wative crystals in heavy atom solutions, in the presence or in the absence of W18, as dictated by the stability of the crystals.

Site Targeting. Tetrakis(acetoxymercuri)-methane (TAMM) was covalently bound to exposed SH^- groups as described for the tetrairidium cluster in (24). TAMM mercuration of cDNA oligomers was performed on 5′ extensions of the oligomers containing thiolated bases. The non-oligomer-bound mercury atoms of the TAMM molecule were masked to avoid the attachment of the oligomers to undesired locations as described (11). The oligomer presented in these studies was (AGAAAG-GAGGTGATC), to which a tail of A(thio-dG)$_3$ was added.

Data Collection and Evaluation. Data were collected with a bright synchrotron beam at cryotemperature (86–90 K) from flash frozen crystals, as described (23). The data were recorded either on the 345 mm MAR Research (Hamburg) or charge-coupled device detectors [QUANTUM4 or APS2, Cornell High Energy Syncrotron Source (CHESS), Ithaca, NY] and were processed by HKL2000 (25). For anomalous data collection, the wavelength was adjusted to the L_3 edge of W. Collecting the 3–4 Å shell, decay was detected within a period sufficient for 1–1.5° oscillations. To facilitate the production of complete data sets, crystals were irradiated by a beam with a smaller cross-section. Translating the rod-like crystals (≈500 × 60 × 60 microns) once decay was observed allowed measurements from 2–6 separate regions. Larger cross sections were chosen when a less intense or divergent beam was provided. Under these conditions, however, only lower resolution data (<5–6 Å) could be collected.

Phasing. Because the original native crystals (5) became obsolete by the W18 treatment, Wative or BS crystals were considered "native," depending on the given soaking procedure. Data reduction, scaling, and initial phasing were performed with the CCP4 program package (26). The sites of W18 that were removed by the back-soaking procedure were identified in difference Patterson maps, and those that exist in the BS crystals were detected by using anomalous signals. The sites of the additional heavy atoms were determined and verified by difference Patterson and difference Fourier procedures. Refinement and phasing were carried out with the program SHARP (27). Heavy atom clusters, such as W18, Ta_6Br_{14}, tetrairidium, and TAMM were represented by their spherical averaged form factors, as implemented in SHARP (27). The initial 7 Å multiple isomorphous replacement map, obtained by W18 and Ta_6Br_{14}, was subjected to density modification by using the program SOLOMON (28), assuming a solvent content of 65%. The incorporation of phase information from derivatives diffracting to ≈6 Å resulted in a map with Figure of merit = 0.59 and $R_{cullis} = 0.75$. The resolution of the map was extended to 4.5 Å in steps by the incorporation of phase information from additional heavy atom derivatives (Table 1). After tracing of ≈500 nucleotides, the model, ac-

BIOCHEMISTRY

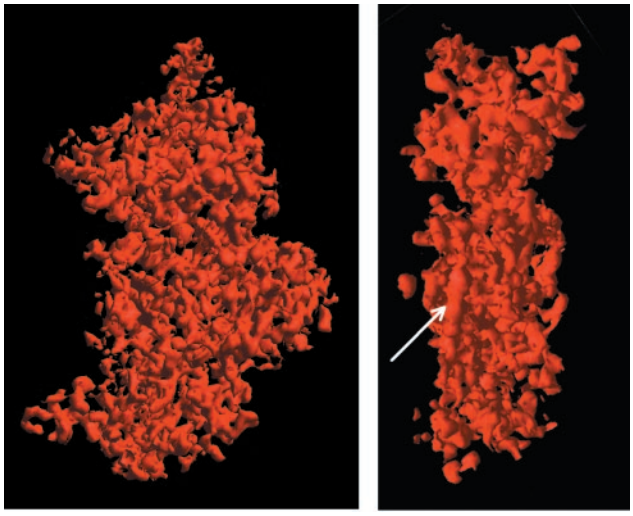

Fig. 1. Two orthogonal views of the overall structure of the small subunit, as extracted from the 4.5 Å map (contour level 1.2 SD). The arrow points at an exceptionally long dense region, suitable to host double-helical RNA chain that may be interpreted as helix 44 in the model of the 16S RNA (18).

counting for ≈28% of the total mass, was subjected to rigid-body refinement. The phases generated from the refined positions were combined with those originating by multiple isomorphous replacement. This step was carefully monitored by the introduction of several weighing procedures, as well as by the temporary removal of parts of the model used for phase combination.

Map Interpretation. Fitting was carried out by following the features of the map. Building blocks were constructed from known RNA motifs (canonical RNA A-form, hammer head, anticodon loop, sarcin/ricin loop, archaeal bulge-helix-bulge, pseudoknot, specific kinks and turns, etc.) or from the ribosomal proteins whose structures have been determined crystallographically or by NMR (20, 21). Tracing was performed interactively, using the program O (29). The results were displayed either by O or by RIBBONS (30).

Results and Discussion

The initial 7 Å as well as the current 4.5 Å maps contain shapes with a morphology remarkably similar to most of the cryoelectron microscopy reconstructions (1, 2, 12, 13) of small ribosomal subunits. They show the consensus division into a "head" connected by a short "neck" to a bulky lower "body" (Fig. 1) and contain elongated dense features alongside lower-density globular regions.

The 7 Å resolution map was found suitable for initial fittings of both RNA chains and protein structures. At around 6 Å, the number of the RNA duplexes that appeared as separated chains became larger. At 4.5 Å, a larger number of regions suggesting

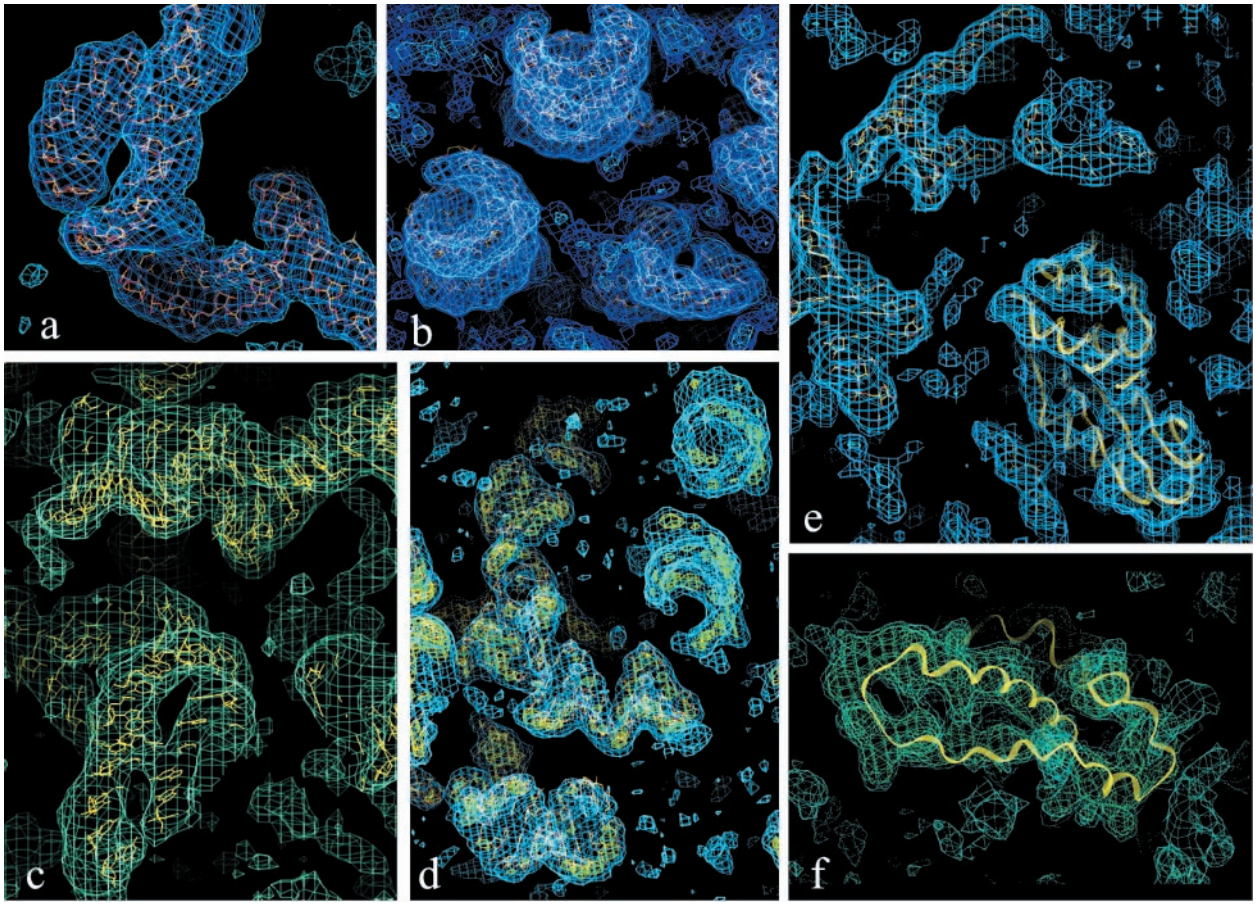

Fig. 2. Parts of the T30S electron density maps at different stages of structure determination from 6 to 4.5 Å (contour level 1 SD, unless otherwise mentioned). (*a*) A helix-bulge-helix region, traced at 6 Å resolution. (*b* and *c*) Views of A-form RNA regions within the 4.5 Å map. (*d*) Part of the 4.5 Å map, contoured at 1.5 (cyan) and 2.5 (green-yellow) SD. These levels were chosen to avoid background noise and to highlight the phosphates in the RNA backbone, respectively. (*e* and *f*) The regions of the 4.5 Å map assigned to protein TS5 and TS15, respectively. In *f*, the less well defined helix was found to be flexible in isolation by NMR and x-ray (21).

prominent protein folds were detected, and the phosphates belonging to the RNA backbone appeared as bulges. Density accounting for the bases could be seen (Fig. 2), but individual bases were still not well resolved, similar to the observations made at comparable resolution in several other systems (31–34). Although the current resolution is too low to suggest novel structural motifs, indications for them were nevertheless detected in the course of map interpretation.

We have previously reported experiments in which tetrairidium attached to exposed cysteines revealed the locations of proteins TS11 and TS13 at 6–7 Å resolution (11, 24). The position of TS13 is compatible with that suggested by immunoelectron microscopy (14), neutron scattering (16), and modeling experiments (19). However, the position of the surface of TS11 deviates from the neutron scattering map by a distance larger than the expected diameter of this protein. These results have been confirmed by using TAMM instead of tetrairidium. Furthermore, the availability of a map of a higher detail allowed the examination of the vicinity of the bound heavy atom compounds. It was found that the cysteine of TS13 is located in a region rich in features interpretable as α helices and β sheets whereas the quality of the map in the vicinity of TS11 is somewhat lower.

The structures of ribosomal proteins that have been determined crystallographically or by NMR (20, 21) were exploited for visual placements, keeping in mind that these assignments are only partially justified. Guidelines were taken from the large volume of noncrystallographic studies. In these experiments, proteins TS5 and TS7 (Fig. 2) were found to be in the vicinity of the positions suggested for them by earlier noncrystallographic studies (14, 16, 19). The case of protein TS15 is more complicated because several regions suitable to accommodate its core could be identified in the map. As the core of protein S15 contains well packed α helices (reviewed in refs. 20 and 21), a structural element that is likely to be common among ribosomal proteins, this finding was not surprising. In neither of the potential positions of protein S15, the remaining part of this protein, a flexible arm, could be well placed (Fig. 2). All of these positions are rather far from the location of S15 in the neutron scattering map (16). Hence, the region closest to the location of S15 in the neutron density map was tentatively chosen (Fig. 3). It is noteworthy that several additional regions suitable to accommodate ribosomal proteins were identified but still not assigned. Of interest is a region that seems to be rich in loosely packed α helices, located at the protein-free part of the neutron scattering map (16), at the bottom of the particle.

Hybridization of exposed RNA regions with mercurated cDNA oligomers was found to be useful for independent site identifications as well as for monitoring ribosomal functional activities. The following example is illuminating. The oligomer complementary to the 3′ end of the 16S RNA (called here oliT) was found to hybridizes well even as its TAMM mercurated form. Furthermore, despite its large-size, which may reach 70 Å in length, it readily diffused into the crystals that were found to diffract to resolutions comparable to that of the Wative or BS crystals. Indications for the location of its mercurated tail were obtained first at 7.5 Å resolution (11). Extending these studies to the current resolution allowed an analysis of the vicinity of this site, which, as expected, contains a rather long single stranded RNA chain (Fig. 3). It also led to more accurate positioning of the 5′ end of the cDNA oligomer.

This oligomer is of high functional relevance, as it contains the Shine-dalgarno sequence, thus imitating the mRNA segment involved in the initiation of protein biosynthesis. It was designed to dock at the 3′ end of the 16S RNA that contains the anti-Shine-Dalgarno sequence, and to mimic the formation of the initiation complex. This region of the 16S chain is known to be rather flexible and may adopt several conformations (19). Hence, it is suggested that the high quality diffraction obtained from the crystals derivatized by this oligomer results from stabilization of the flexible 3′ arm of the 16S RNA in a fashion that mimics its binding to mRNA.

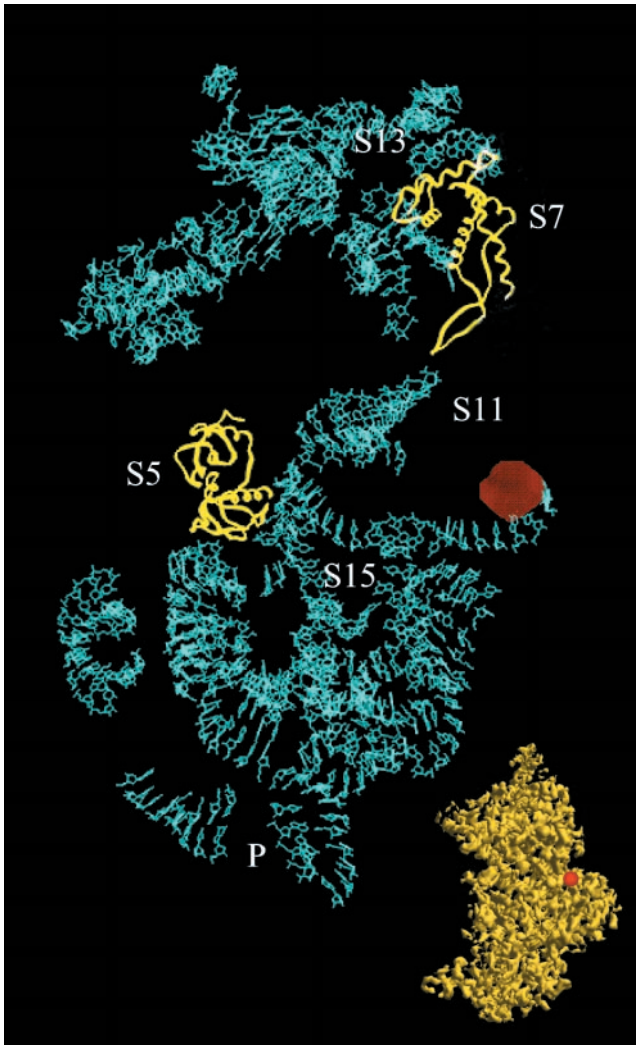

Fig. 3. Most of the so far traced RNA chain (in cyan). The position of the center of mass of the TAMM molecules that were bound to the mRNA analog is shown as a red sphere (of artificially enlarged size). The locations of proteins TS5, TS7 are represented by their backbone structure, as determined crystallographically. The tentative locations of the center of protein TS15 and of the exposed cysteines of proteins TS11 and TS13 are marked by their numbers. P shows a possible location for a still-not-assigned protein. For orientation, the oliT position has been placed on the body of T30S subunit (shown in the lower-right insert).

It is still premature to determine whether the site revealed in the current map reflects the position of the 3′ end of 16S RNA at its free, 50S bound, or intermediate conformations. Interestingly, the position assigned for the 5′ end of this oligomer was found to be at close proximity to one of the major sites of W18. Because both the polyanion cluster and the RNA chains are negatively charged, it is conceivable that their interactions are mediated by Mg^{2+} ions. Regardless of the mode of the interactions, it is likely that the gain of resolution by the W18 treatment is a result of minimizing the flexibility of the RNA chains. Indeed, so far, all W18 sites were detected in positions that may significantly reduce the mobility of the T30S particles within the crystal network. Thus, two of the main W18 sites were detected at the interface between the two paired particles, indicating a possible involvement of W18 in the pairing contacts.

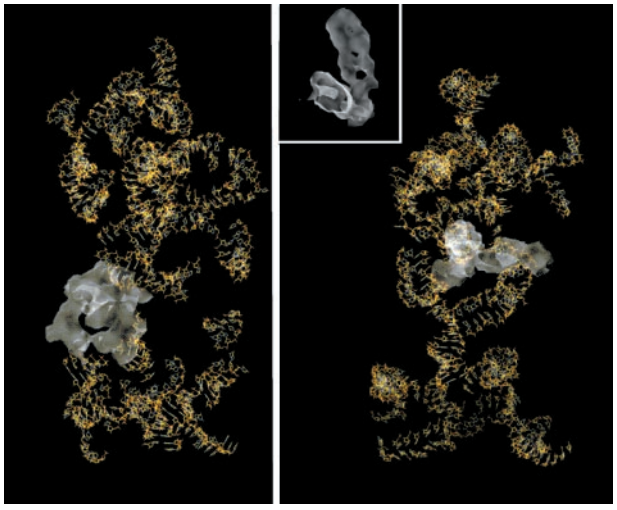

Fig. 4. The regions that became interpretable by the incorporation of the anomalous data, shown as white objects. The insert focuses on one of them, traced later as helix-bulge-helix motif.

To gain confidence in the 4.5 Å map, it was screened for structural features that were not detected in the lower resolution maps. Among those, a prominent spherical object of a size comparable to that of the W18 cluster was clearly seen. Also, the contribution of the W anomalous signals provided additional verification for the quality of both the multiple isomorphous replacement and the multiple isomorphous replacement with anomalous signals maps, as it led to marked improvement in several regions, two of which are shown in Fig. 4. Finally, several portions of the modeled RNA chain were removed before its use for phase combination, and the map resulting from the combined phases was examined. Some variability in map quality was evident. Nevertheless, in many positions, considerable improvement in the map was detected (Fig. 5), and RNA regions that were not used in the phase combination procedure could be clearly visualized.

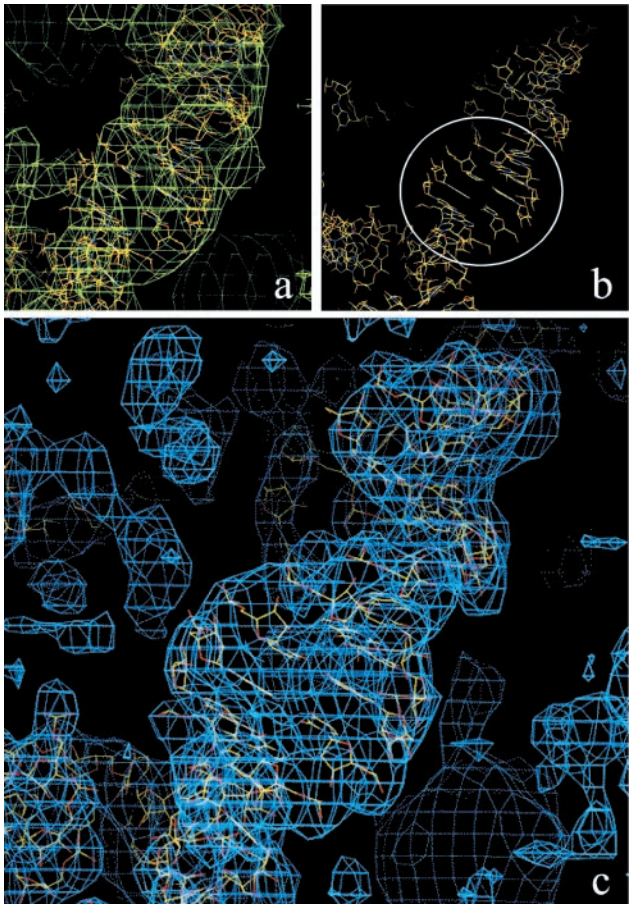

Fig. 5. (*a*) A region of the 7 Å map and its interpretation before phase combination. The portion of the modeled RNA that was removed before phase combination (highlighted by a circle). (*c*) The comparable part of the phase-combined 5 Å map, showing the features detected at the surroundings of the removed part.

Conclusions

The unbiased structural information revealed in this study is consistent with most of the available noncrystallographic data, but at the same time it presents some deviations. Careful inspection of the current map resulted in the identification of a wealth of commonly occurring as well as rarely found structural elements. However, it is clear that, at this stage, detailed functional assignments are bound to depend heavily on models created according to biochemical and biophysical considerations. Because we have shown that selected ribosomal sites can be targeted within the crystals, and because data are being collected to higher resolution, there are solid reasons to expect that a reliable and unbiased interpretation, capable of shedding light on intricate functional issues, will soon emerge.

Note. Two related crystallographic studies, albeit performed at lower resolution, were published during the reviewing period of this manuscript. These report assignments of ribosomal components within maps of the small (35) and the large (36) subunit, in a fashion based exclusively on the existing noncrystallographic ribosomal models. Interestingly, the upper part of the 5.5 Å small subunit structure (35) appears to be less well resolved, compared with that reported here. This may be attributable to the postcrystallization activation step used by us.

We thank M. Wilchek for indispensable advice, M. Pope, W. Jahn, and W. Preetz for heavy atom compounds, M. Safro and I. Levin for active participation, R. Brimacombe and F. Müller for the 16S model, W. Traub for fruitful discussions, and R. Albrecht, T. Auerbach, H. Avila, W. S. Bennett, H. Burmeister, C. Glotz, Y. Halfon, M. Kessler, K. Knaack, M. Laschever, S. Meier, J. Müssig, M. Pioletti, M. Peretz, C. Radzwill, M. Simitsopoulou, S. Weinstein, and R. Zarivach for contributing to different stages of these studies, and to the synchrotron radiation facilities staff: European Molecular Biology Laboratory and Max Planck Group beam lines at Deutsches Elektronen Synchrotron; F1/Cornell High Energy Syncrotron Source; ID2 and ID13 at the European Syncrotron Radiation Facility; and ID19/APS at Argonne National Laboratory. Support was provided by the Max-Planck Society, the National Institutes of Health (Grant GM 34360), the German Ministry for Science and Technology (Bundesministerium für Bildung, Wissenschaft, Forschung und Technologie Grant 05-641EA), and the Kimmelman Center for Macromolecular Assembly at the Weizmann Institute. A.Y. holds the Martin S. Kimmel Professorial Chair.

1. Harms, J., Tocilj, A., Levin, I., Agmon, I., Stark, H., Kolln, I., van Heel, M., Cuff, M., Schlunzen, F., Bashan, A., *et al.* (1999) *Structure Fold. Des.* **7,** 931–941.
2. Gabashivili, I. S., Agrawal, R. K., Grassucci, R. & Frank, J. (1999) *J. Mol. Biol.* **286,** 1285–1291.
3. Wang, R., Alexander, R. W., VanLoock, M., Vladimirov, S., Bukhtiyarov, Y., Harvey, S. C. & Cooperman, B. S. (1999) *J. Mol. Biol.* **286,** 521–540.
4. Tapprich, W. E. & Hill, W. E. (1986) *Proc. Natl. Acad. Sci. USA* **83,** 556–560.
5. Yonath, A., Glotz, C., Gewitz, H. S., Bartels, K., von Boehlen, K., Makowski, I. & Wittmann, H. G. (1988) *J. Mol. Biol.* **203,** 831–833.
6. Trakhanov, S. D., Yusupov, M. M., Agalarov, S. C., Garber, M. B., Ryazantsev, S. N., Tischenko, S. V. & Shirokov, U. A. (1987) *FEBS Lett.* **220,** 319–322.

7. Ban, N., Freeborn, B., Nissen, P., Penczek, P., Grassucci, R. A., Sweet, R., Frank, F., Moore P. & Steitz, T. (1998) *Cell* **93,** 1105–1115.
8. Dawson, B. (1953) *Acta Crystallogr.* **6,** 113–126.
9. Yonath, A., Harms, J., Hansen, H. A., Bashan, A., Schlunzen, F., Levin, I., Koelln, I., Tocilj, A., Agmon, I., Peretz, M., *et al.* (1998) *Acta Crystallogr. A* **54,** 945–955.
10. Zamir, A., Miskin, R. & Elson, D. (1971) *J. Mol. Biol.* **60,** 347–364.
11. Auerbach, T., Pioletti, M., Avila, H., Anagnostopoulos, K., Weinstein S., Franceschi, F. & Yonath, A. (1999) *Biomol. Struct. Dyn.*, in press.
12. Stark, H., Mueller, F., Orlova, E. V., Schatz, M., Dube, P., Erdemir, T., Zemlin, F., Brimacombe, R. & van Heel, M. (1995) *Structure (London)* **3,** 815–821.
13. Frank, J., Zhu, J., Penczek, P., Li, Y., Srivastava, S., Verschoor, A., Radermacher, M., Grassucci, R., Lata, A. R & Agrawal, R. K. (1995) *Nature (London)* **376,** 441–444.
14. Stöffler, G. & Stöffler-Meilicke, M. (1986) in *Structure, Function and Genetics of Ribosomes*, eds. Hardesty, B. & Kramer, G. (Springer, Heidelberg), pp. 28–46.
15. Oakes, M. I., Clark, M. W., Henderson, E. & Lake, J. A., (1986) *Proc. Natl. Acad. Sci. USA* **83,** 275–279.
16. Moore, P. B., Capel, M. S., Kjeldgaard, M. & Engelman, D. M. (1985) in *Structure, Function and Genetics of Ribosomes*, eds. Hardesty, B. & Kramer, G. (Springer, Heidelberg), pp. 87–100.
17. Merryman, C., Moazed, D., McWhirter, J. & Noller, H. F. (1999) *J. Mol. Biol.* **285,** 97–105.
18. Malhotra, A. & Harvey, S. C. (1994) *J. Mol. Biol.* **240,** 308–340.
19. Müller, F. & Brimacombe, R. (1997) *J. Mol. Biol.* **271,** 524–544.
20. Liljas, A. & Al-Karadaghi, S. (1997) *Nat. Struct. Biol.* **4,** 767–771.
21. Ramakrishnan, V. & White, S. W (1998) *Trends Biochem. Sci.* **3,** 208–212.
22. Nyborg, J., Nissen, P., Kjeldgaard, M., Thirup, S., Polekhina, G., Clark, B. F. C. & Reshetnikova, L. (1996) *Trends Biochem. Sci.* **21,** 81–82.
23. Schlünzen, F., Koelln, I., Janell, D., Gluehmann, M., Levin, I., Bashan, A., Harms, J., Bartels, H., Auerbach, T., Pioletti, *et al.* (1999) *J. Synth. Radiation* **6,** 928–941.
24. Weinstein, S., Jahn, W., Glotz, C., Schluenzen, F., Levin I., Janell, D., Harms, J., Kolln, I., Mansen, H. A. S., Gluehmann, M., *et al.* (1999) *J. Struct. Biol.* **127,** 141–151.
25. Otwinowski Z. & Minor, W. (1997) *Methods Enzymol.* **276,** 307–326.
26. CCP4 Collaborative Computational Project (1994) *Acta Crystallogr. D* **50,** 760–763.
27. La Fortelle E. & de Bricogne, G. (1997) *Methods Enzymol.* **276,** 472–494.
28. Abrahams, J. P. & Leslie, A. G. W. (1996) *Acta Crystallogr. D* **52,** 30–42.
29. Jones, T. A., Zou, J.-Y., Cowan, S. W. & Kjeldgaard, M. (1991) *Acta Crystallogr. A* **47,** 110–119.
30. Carson, M. (1991) *J. Appl. Crystallogr.* **24,** 958–961.
31. Wolberger, C., Ding, Y., Ptashne, M. & Harrison, S. H. (1988) *Nature (London)* **335,** 789–795.
32. Jaeger, J., Restle, T. & Steitz, T. A. (1998) *EMBO J.* **17,** 4535–4542.
33. Price, S., Cusack, S., Borel, F., Berthetcolominas, C. & Leberman, R. (1993) *FEBS Lett.* **324,**167–170.
34. Golden, B., Gooding, A. R., Podell, E. R. & Cech, T. A. (1998) *Science* **282,** 259–264.
35. Clemons, W. M., Jr., May, J. L., Wimberly, B. T., McCutcheon, J. P., Capel, M. S. & Ramakrishnan, V. (1999) *Nature (London)* **400,** 833–840.
36. Ban, N., Nissen, P., Hansen, J., Capel, M., Moore, P. B. & Steitz, T. A. *Nature (London)* **400,** 841–847.